ACS APPLIED MATERIALS & INTERFACES

Research Article

www.acsami.org

Cytotoxicity and Gene Expression in Sarcoma 180 Cells in Response to Spiky Magnetoplasmonic Supraparticles

Hongjian Zhou,[†,∥] Sun Il Choi,[‡,∥,⊥] Fengming Zou,[§] Sangjin Oh,[†] Ji Eun Kim,[‡] Dae Youn Hwang,*[,‡] and Jaebeom Lee*[,†]

[†]Department of Nano Fusion, and Cogno-Mechatronics Engineering, Pusan National University, Busan 609-735, Republic of Korea

[‡]Department of Biomaterials Science, College of Natural Resources and Life Science, Pusan National University, Miryang 627-706, Republic of Korea

[§]Department of Nano Fusion Technology and BK21 Plus Nano Convergence Technology Division, Pusan National University, Busan 609-735, Republic of Korea

Supporting Information

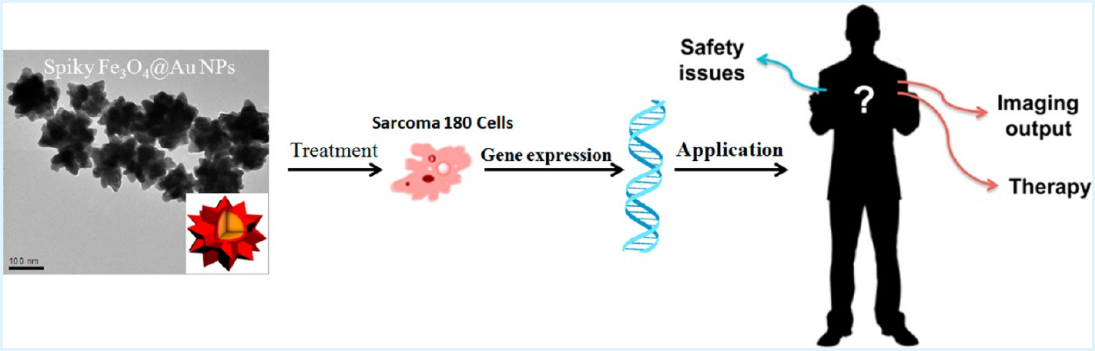

ABSTRACT: Multifunctional nanoparticles (NPs) have been designed for a variety of cell imaging and therapeutic applications, and the study of their cellular interactions is crucial to the development of more efficient biomedical applications. Among current nanomaterials, concave core−shell NPs with complex angled geometries are attractive owing to their unique shape-dependent optical and physical properties as well as different tendency for cell interaction. In this study, we investigated the morphology effect of spiky gold-coated iron oxide supraparticles (Fe_3O_4@Au SPs) on cytotoxicity and global gene expression in sarcoma 180 cells. Cells treated for 7 days with spiky supraparticles (SPs) at concentrations up to 50 μg/mL showed >90% viability, indicating that these NPs were nontoxic. To shed light on the differences in cytotoxicity, we monitored the expression of 33 315 genes using microarray analysis of SP-treated cells. The 171 up-regulated genes and 181 down-regulated genes in spiky SP-treated cells included *Il1b*, *Spp1*, *Il18*, *Rbp4*, and *Il11ra1*, where these genes are mainly involved in cell proliferation, differentiation, and apoptosis. These results suggested that the spiky Fe_3O_4@Au SPs can induce noncytotoxicity and gene expression in tumor cells, which may be a promising cornerstone on which to base related research such as cyto-/genotoxicology of nanomaterials or the design of nanoscale drug carriers.

KEYWORDS: *concave core−shell nanoparticle, tumor cell, cytotoxicity, microarray, gene expression*

1. INTRODUCTION

It is fundamental to understand the interaction between multifunctional nanoparticles (NPs) and the cell for its application on cell image and therapeutics.[1−3] The mutual reaction between cells and NPs varies with the surface properties of NPs, including composition, morphology, size, shape, and ionic strength.[4,5] The surface morphology of NPs plays the most important role in the cellular interactions and systemic distribution of NPs.[6−12] For example, cytotoxicity of gold NPs is well studied under different surface coating and shape (nanoparticle, nanoshells, and nanorods). The studies showed that the cell viability was not reduced by gold nanoshells compared to control cells.[13] Moreover, spherical gold NPs with the same surface functionalization are generally more toxic and more efficiently uptaken than rod-shaped particles.[14] A few researches focus on the cytotoxicity of concave metallic NPs.

Recently, increasing attention has been paid to the fabrication of concave metallic NPs.[15−24] Distinctively, Au-coated iron oxide (Fe_3O_4@Au) NPs have been the focus of study owing to their intriguing bifunctional (magnetic and optical) properties.[25,26] Anisotropic Au NPs can support large optical cross sections at near-infrared wavelengths and are easy to do optical imaging modalities for their high rates of transmission through biological tissues.[27−29] Moreover, Fe_3O_4 NPs are useful

Received: July 15, 2014
Accepted: November 4, 2014
Published: November 4, 2014

as T_2-weighted contrast agents in magnetic resonance imaging and are able to react to magnetic field gradients applied to site-specific localization (e.g., magnetofection) or separation (e.g., cell sorting).[30] Most importantly, the magnetic and plasmonic properties in the hybrid structures can affect each other in current work which is called magnetoplasmonics.[31] As a multifunctional magnetoplasmonic nanomaterial, the special optical properties and superparamagnetic properties that NPs inherit from these two components would highly improve and broaden the application as multifunctional nanocomposites.

Indeed, due to their multifunctionality in surface modification, superparamagnetic, and optical properties such as localized surface plasmon resonance and surface-enhanced Raman scattering, Fe_3O_4@Au nanostructures have been recently applied in biomedical fields, like drug delivery systems,[32,33] bioanalysis,[34,35] imaging,[36] and disease detection/therapy.[37,38] The importance of the surface morphology of Fe_3O_4@Au NPs in the design of high-performance delivery systems for therapeutic drugs has been increased in order to examine the effect of particle morphology on cellular functions using bioinformatic methods up to gene expression.[39] Profiling of gene expression is a forceful tool to evaluate the mechanism of cell response to any external stimuli that results in transcriptional changes. Gene regulation can be figured out through a variety of methods,[40,41] and it can simultaneously determine the expression of thousands of genes which occur in disease,[42] even in its early period or in response to pharmacological[43] or toxicological stimuli. Even simple experiments will produce large amounts of data, and thereby expression profiling through the experiments can revolutionize our understanding of many cellular processes. Expression monitoring is also a powerful means in the pharmaceutical industry such as drug discovery, medicinal development, medical setting, medical diagnosis, and clinical surveillance. Gene expression monitoring related to toxicology is expected to make extraordinary contributions.[44] Detailed transcriptional responses to toxic stress will be helpful for us to comprehend the effects of toxic compounds, which will enable us to design better strategies for safer nanomaterials.

We previously reported a unique metallic core−shell nanocomplex, i.e., spiky gold-coated iron oxide supraparticles (Fe_3O_4@Au SPs) with diameters of 105−185 nm and strong magnetization using the self-assembly method, which has drawn considerable attention because of their unique surface morphology and electromagnetic bifunctionality.[45]Inorganic superclusters—which are also called "supraparticles (SPs)" because they can assemble technically—are an emerging and hot research topic in many research fields, such as chemistry, physics, and materials science.[31,46] They exhibit unique physiochemical properties due to their well-defined shape and distinctive topological structure.[47] Therefore, in this article we investigated their cytotoxicity in detail by using mouse sarcoma 180 tumor cells to obtain fundamental information on nanoscale toxicity before we carry out different biomedical applications. Furthermore, we used microarray analysis to demonstrate the potential effects of spiky SPs on cell differentiation, cell proliferation, cell cycle, immune response, apoptosis, and signal transduction. These bioinformatics approaches will shed light on the effects of nanoscale differences in shape on cellular responses and provide fundamental information for the development of further therapeutic nanocomplexes.

2. EXPERIMENTAL SECTION

Materials. Gold(III) cloride hydrate ($HAuCl_4$, 99.9%), sodium citrate ($Na_3C_6H_5O_7$), iron(III) chloride ($FeCl_3$), hydroquinone (98%), and 28% ammonium hydroxide solution (NH_4OH) were obtained from Sigma-Aldrich (Milwaukee, USA). Iron(II) chloride ($FeCl_2$) was purchased from Wako Pure Chemical Industries Ltd. (Tokyo, Japan). Deionized water (>18.2 mΩ/cm) was used throughout the experiment. All chemicals were of analytical grade without any further purification. Sarcoma 180 cells, a murine tumor cell line, were obtained from the American Type Culture Collection (Rockville, MD, USA). All cells were maintained in a humidified incubator at 37 °C and 5% CO_2. Fetal bovine serum, penicillin, and streptomycin for cell cultures were purchased from Hyclone Laboratories Inc. (Logan, UT, USA).

Synthesis of Fe_3O_4 Magnetic NPs. Iron oxide nanoparticles (Fe_3O_4 NPs) were prepared through the coprecipitation method.[45] Typically, 1.622 g of $FeCl_3{\cdot}6H_2O$ and 0.994 g of $FeCl_2{\cdot}4H_2O$ were dissolved in 40 mL of water with magnetic stirring. After that, 5 mL of 25% NH_4OH was injected quickly to the reaction solution and allowed to stand for 10 min. Next, 4.4 g of sodium citrate was added to this reaction mixture under 90 °C for 30 min with stirring. Then the mixture was cooled to room temperature and thoroughly rinsed with ethyl alcohol several times. In rinsing, samples were separated from the supernatant by a permanent magnet. Finally, the black precipitates were dried under room temperature in vacuum.

Preparation of Spherical Au-Coated Iron Oxide (Fe_3O_4@Au) Seed. Au-shell coating was performed by reducing Au^{3+} on the surface of Fe_3O_4 NPs via the modification of a method described in our previously published study.[49] Briefly, 20 mL of 0.5 mM $HAuCl_4$ solution was heated until boiling with vigorous stirring. Rapidly injecting 10 mL of Fe_3O_4 solution resulted in the formation of Fe_3O_4@Au NPs; heating was continued for another 10 min; next, we removed the heating plate and cooled the solution to room temperature with stirring. The Fe_3O_4@Au NPs were obtained after 3 times of centrifugation at 6500 rpm for 20 min. Finally, the nanoparticles were redispersed in 10 mL of deionized water. The final Fe_3O_4@Au NP seed solution showed dark purple color.

Preparation of Spiky Fe_3O_4@Au SPs. Spiky Au-shell coating was achieved via reduction of Au^{3+} on the surface of spherical Fe_3O_4@Au seed by the self-assembly method in our previous publication.[45] Typically, 10 mL of $HAuCl_4$ (0.25 mM) solution was made under magnetic stirring, and then, 100 μL of Fe_3O_4@Au seeds and 1 mL of hydroquinone (30 mM) were added into the $HAuCl_4$ solution. The reaction solution was stirred under room temperature for 30 min. The final spiky Fe_3O_4@Au SPs solution showed green color.

Fluorescence-Activated Cell Sorting (FACS) Analysis of Sarcoma 180 Cells to Fe_3O_4 Magnetic NPs. Flow cytometry was performed on a FACS Calibur (MuseTM Cell Analyzer, EMD Millipore, Germany). Sarcoma 180 cells (7×10^6/well) were cultured overnight on six-well cell culture plates in RPMI medium containing 10% of fetal bovine serum, 100 IU/mL of penicillin, and 100 μg/mL of streptomycin. When the cells reached 70−80% confluence, they were exposed to deionized water (control) and various concentrations of Fe_3O_4 magnetic NPs (0.75, 1.5, 3.15, 6.3, 12.5, 25, and 50 μg/mL) for 7 days. Cells were harvested using trypsinization and 100 μL of cell suspensions for 20 min using MuseTM Annexin-V & Dead Cell reagent in the darkness. Then, the Annexin-V/7-AAD positive cells were quantitatively detected with a MuseTM Cell Analyzer (Merck-Millipore, Germany). Annexin-V stained cells were only marked for early apoptotic and cells double-stained with Annexin-V and 7-ADD were marked for late apoptotic.

Cell Culture and Cell Viability Assay. Cell viability was determined indirectly using the tetrazolium compound MTT (Sigma-Aldrich, Korea). Briefly, sarcoma 180 cells were seeded at 200 cells/μL density in 96-well plates and incubated in a carbon dioxide incubator for 24 h at 37 °C. After 70−80% confluence of cells was achieved, the cells were exposed to different concentrations of spiky SPs (0, 0.79, 1.58, 3.17, 6.25, 12.5, 25, and 50 μg/mL) for 7 days. Two groups of cells were prepared for comparison of cytotoxicity and gene expression—namely, a deionized water-treated group as a control

(vehicle) and spiky groups. After the supernatants of sarcoma 180 cells were removed, fresh RPMI 1640 medium (200 μL, 2 mg/mL in PBS solution) and MTT solutions (50 μL, 2 mg/mL in PBS solution) were injected to the control and spiky groups. After that, the cells were incubated at 37 °C. The viable cells were determined to convert the soluble MTT into an insoluble purple formazan precipitate in a 220 μL sample of control and spiky groups in 4 h. The formazan precipitate was quantified by measuring the absorbance at 570 nm using a spectrophotometer (Molecular Devices, Sunnyvale, CA, USA).

Transmission Electron Microscopy (TEM) of Spiky SP-Treated Cells. The intracellular ultrastructure of sarcoma 180 cells treated with increasing concentration (0−50 μg/mL) of spiky SPs was observed after 24 h of incubation by transmission electronic microscopy (TEM). After treatment using spiky SPs, the cells (1×10^6 cells) were washed with PBS buffer three times and then with 2.5% of glutaraldehyde and 1% of osmuim tetroxide at 4 °C in 7.2 PBS solution. The fixed cell cultures were dehydrated using graded ethyl alcohol and finally embedded by covering with a layer of epoxy resin (Epon 812 mixture). Ultrathin sections (50−60 nm) were obtained using an ultramicrotome (EM UC7, Leica) and contrasted with uranyl acetate and lead citrate. Finally, the thin sections were observed using an electron microscope (H-7600, Hitachi, Japan) at 80 kV.

Microarray Analysis. RNA was extracted using an RNA-Bee solution (Tel-Test, Austin, TX, USA). To control and test RNAs, we synthesized and hybridized target complementary RNA (cRNA) probes using a low-RNA input linear amplification kit (Agilent Technology, USA). The process was performed as Jong Kun Park reported.[50]

Data Acquisition and Analysis. All data and hybridized images obtained from Microarray assays were analyzed based on Hyo-Eun Kim's report.[51]

RESULTS

Preparation of Spiky Fe_3O_4@Au SPs. We designed spiky Fe_3O_4@Au core−shell SPs with multifunctional properties using the self-assembly approach.[45,49] Citrate-coated Fe_3O_4 NPs are initially prepared as the central cores in an aqueous state. They are subsequently coated with Au layers via reduction of $HAuCl_4$ on the citrate on the Fe_3O_4 surface. Then, using synthesized spherical Fe_3O_4@Au NPs as seed, the spiky Fe_3O_4@Au SPs were produced via the self-assembly of additional Au NPs through seed-mediated reduction of $HAuCl_4$ with hydroquinone. Figure 1 presents the transmission electron microscopy (TEM) images of Fe_3O_4 core NPs, spherical Fe_3O_4@Au seed, and spiky Fe_3O_4@Au SPs. On the basis of micrographs from multiple areas, Fe_3O_4 NPs appear to be almost spherical with a diameter of ∼10 nm (as shown in Figure 1A and B). Next, 10 mL of Fe_3O_4 NP solution was added to hydrogen tetrachloroaurate (III) ($HAuCl_4$) solution, yielding Fe_3O_4@Au NPs with high monodispersity. In Figure 1C and D, Au is fully covered on the magnetic core, and the spherical Fe_3O_4@Au seeds are approximately 25 nm in diameter. Figure 1E and F show spiky Fe_3O_4@Au SPs with multiple branches after 1 mL of hydroquinone and 100 μL of Fe_3O_4@Au seeds were added into the reaction system. The number of branches was carefully counted in the TEM images and was approximately 25−30 per NP. Each branch was a cone shape with (111) direction of epitaxial growth and a height of 30 nm; the bottom and top diameters were ∼25 and ∼5 nm, respectively. The average size of the spiky Fe_3O_4@Au SPs was 165 nm. Figure S4 (Supporting Information) shows the Fourier transform infrared spectra of sodium citrate and spiky Fe_3O_4@Au SPs. The 1578 cm^{-1} peak attributed to the C═O stretching vibration from the COOH group of citrate shifts to an intense band at about 1560 cm^{-1} for spiky Fe_3O_4@Au SPs.

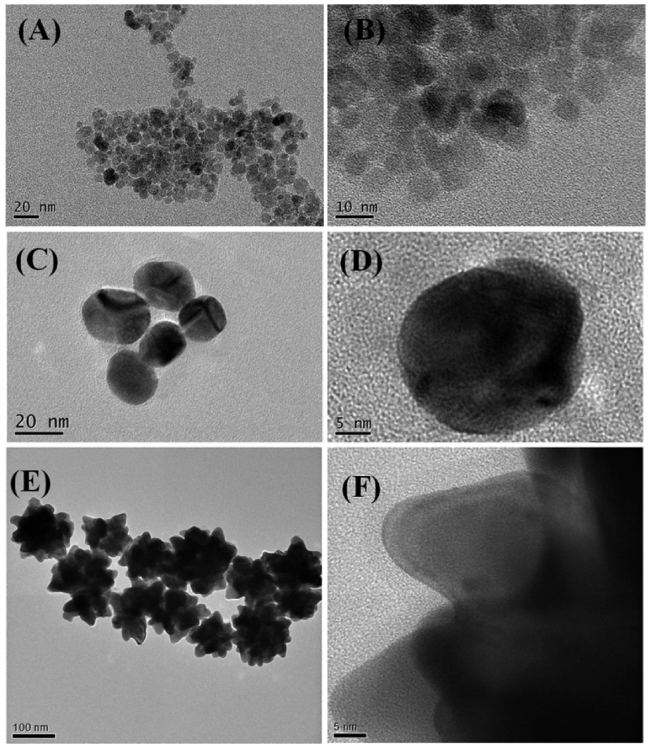

Figure 1. Transmission electron microscopy (TEM) images of (A, B) Fe_3O_4 core NPs, (C, D) spherical Fe_3O_4@Au seeds, and (E, F) spiky Fe_3O_4@Au SPs.

It demonstrated citrate's bonding on the surface of spiky Fe_3O_4@Au SPs by chemisorptions.

Spiky Fe_3O_4@Au SP Effect on Cell Morphology. After exposure to toxic materials, the most noticeable change of cell is its shape or morphology in a monolayer culture. Sarcoma 180 cells, also known as Crocker's tumor, originated in mice as a spontaneous tumor of epithelial lineage. This cell is one of the transplantable, nonmetastasizing, connective tissue tumors of the mouse. Microscopic observations of the treated cells showed no distinct morphological changes between spiky SP-treated groups with different concentrations and the control group. Moreover, microscopic observation of the spiky SP-treated cells showed that the colloidal stability of respective NPs was not changed obviously after the 7 days of treatment, compared with the control group (Figure 2), demonstrating that spiky SPs were nontoxic to sarcoma 180 cells. The whole images depending on culture days (1, 3, 5, and 7 days) can also be seen in Figure S1 (Supporting Information).

Transmission Electron Microscopy (TEM) of Cell Sections. In order to study the biodistribution of the spiky SPs, TEM analyses of the sarcoma 180 cells treated with 25 and 50 μg/mL of spiky SPs were performed. Through endocytosis, such as phagocytosis, pinocytosis, nonspecific endocytosis, receptor-mediated endocytosis (RME), and so on, the nanoparticle can penetrate into the cell.[52] There are no specific ligands on the surface of spiky SPs in our experiment, which suggested that the particles can be permeated into the cell by pinocytosis or nonspecific endocytosis. Untreated cells showed no abnormalities (Figure 3A and B), whereas spiky SP-treated cells showed endosomes near the cell membrane with some nanoparticles inside (Figure 3C and D). We also studied the biodistribution of spiky SPs with high concentration (469 μg/mL) in sarcoma 180 cells. The TEM images were shown in Figure S2

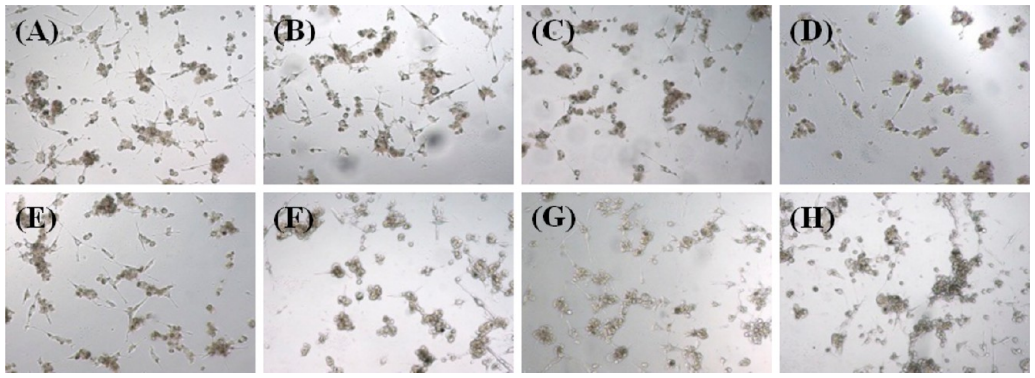

Figure 2. Optical microscopy images (×100) of sarcoma 180 cells exposed to spiky SPs of various concentrations after 7 days: (A) vehicle; (B) 0.79 μg/mL; (C) 1.58 μg/mL; (D) 3.17 μg/mL; (E) 6.25 μg/mL; (F) 12.5 μg/mL; (G) 25.0 μg/mL; and (H) 50.0 μg/mL.

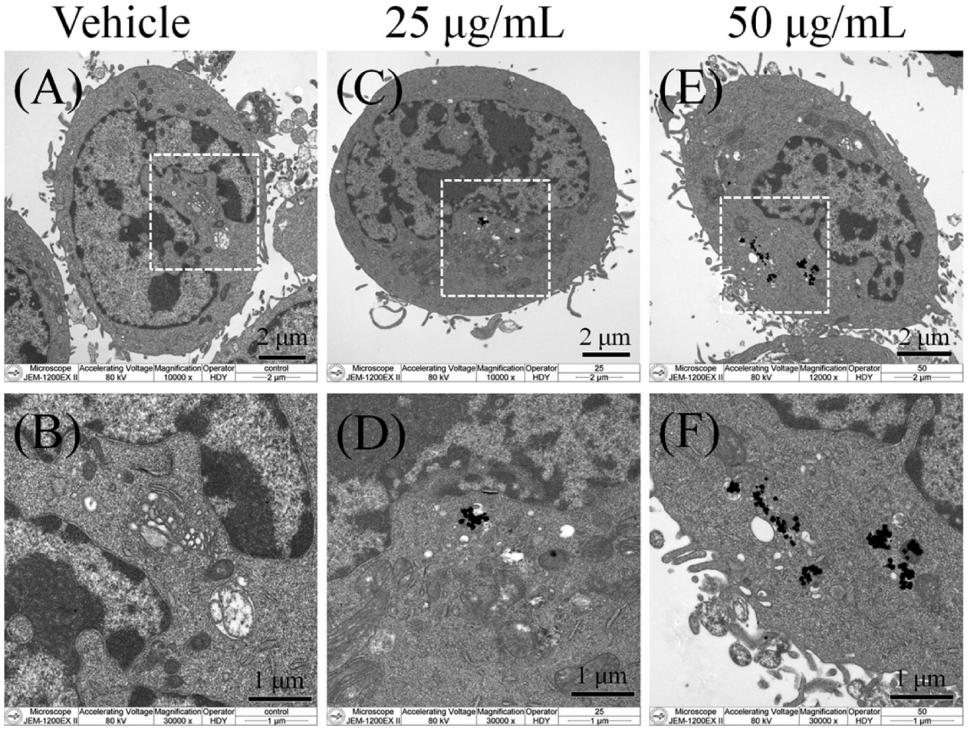

Figure 3. TEM images of sarcoma 180 cells exposed to spiky SPs of various concentrations after 24 h: vehicle (A, B); 25.0 μg/mL (C, D); and 50.0 μg/mL (E, F).

(Supporting Information). We can observe that there is no change in the morphology of sarcoma 180 cells compared with the vehicle group; however, the number of particles permeated into the cell was much higher than 50 μg/mL of the spiky SP group. Therefore, these results demonstrated that 469 μg/mL of spiky SPs was nontoxic to sarcoma 180 cells. The spiky SPs were also found to distribute throughout the cytoplasm, inside lysosomes. Furthermore, spiky SPs were not agglomerated in the cytoplasm (Figure 3D and F). We also observed large endosomes with engulfed spiky SPs in the cytoplasm near the cell membrane (Figure 3F).

The nuclear envelope has multiple pores (nuclear pore complexes) which can transport proteins. Spiky SPs could be easily diffused into the nucleus through the pores owing to their small size. As is shown in Figure S2 (Supporting Information), small vesicles carrying nanoparticles are in contact with invaginations of the nuclear membrane. The cytoplasm exhibited endosomes loaded with heavy nanoparticles, resulting in deposition of spiky SPs in the cytoplasm. A similar mechanism has been reported recently, whereby Au and Ag NPs were engulfed through clathrin- and caveolae-mediated endocytosis in the cell.[53,54] The TEM images demonstrate the endocytic pathway of spiky SP uptake.

Cytotoxicity of Magnetic Core NPs and Spiky SPs. Cell viability analysis was carried out depending on the concentration and culture days. Since the spiky SPs are composed of two different nanomaterials, it is important to validate both materials, i.e., magnetic core NPs and spiky SPs. In particular, it might be possible that the cytotoxicity of the spiky SPs can be swiftly changed because of their unique shape and extraordinary surface areas and charges. The hydroquinone used for branch growth during the synthesis of spiky SPs was eliminated thoroughly before cell experiments. We evaluated the effects of spiky SPs on sarcoma 180 cell viability using an MTT assay. The cytotoxicity profiles of magnetic core NPs and spiky SPs are shown in Figure 4. The cell viability in the presence of

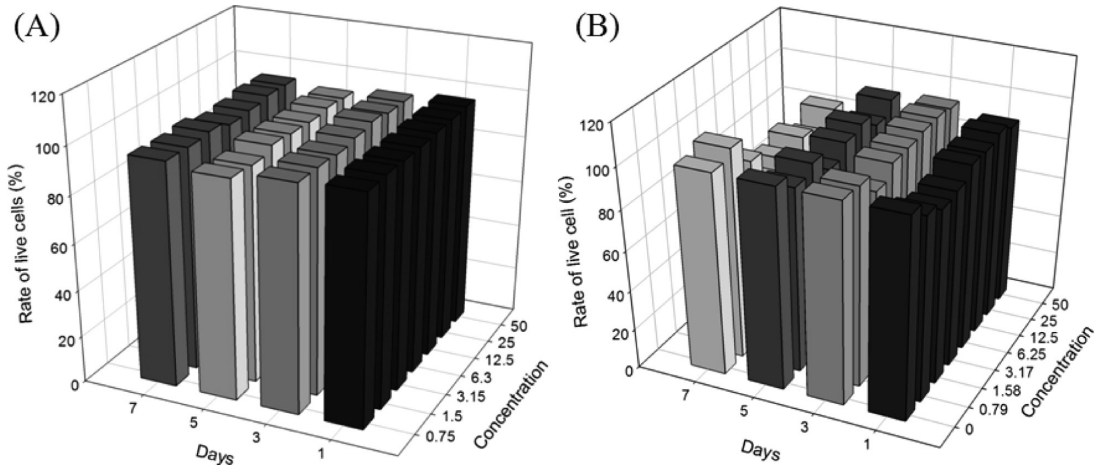

Figure 4. Relative cell viability of sarcoma 180 cells exposed to increasing concentrations (0–50 μg mL^{-1}) of (A) magnetic core NPs and (B) spiky SPs for 7 days.

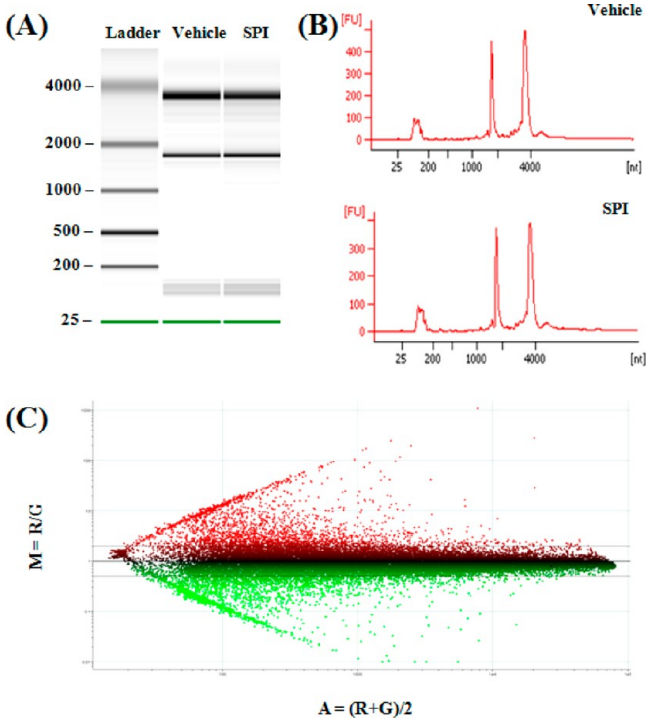

Figure 5. (A) Migration patterns (electrophoretic traces), (B) peak patterns (electropherograms) of the vehicle and the spiky groups, (C) microarray analysis plot summaries of gene expression data on the mouse genome survey, where 33 315 genes were analyzed for the spiky groups: G, green channel; R, red channel.

magnetic core NPs showed no effect on sarcoma 180 cell viability when administered for 7 days (Figure S3, Supporting Information, and Figure 4A). Cells exposed to spiky SPs for 7 days showed >90% viability, indicating that the spiky SPs were nontoxic (Figure 4B). In our observation, the spiky SPs show a little less cell compared with magnetic core NPs. On the basis of this knowledge, noble gold NPs are generally nontoxic due to their inert nature.[55,56] Therefore, our observation suggests that the branched structure of spiky SPs slightly affected the growth of sarcoma 180 cells.

Spiky SP-Mediated Gene Expression Changes in Sarcoma 180 Cells. Changes in global gene expression induced by NPs were investigated to explain the cause of the variance on cell viability at the molecular biology level. First, to verify the quality of total RNA extracted from sarcoma 180 cells, we analyzed the migration and peak patterns of the

Table 1. Functional Classification of Gene up-Regulation and down-Regulation in the Spiky SP-Treated Cells Based on Significantly Represented Gene Ontology Terms[a]

category	term	count
	Up-Regulated Genes	
	signal transduction	40
	cell differentiation	26
	transcription	18
	neurogenesis	13
	cell proliferation	12
	apoptosis	9
	regulation of cellular protein metabolic process	7
	inflammatory response	6
	immune response	6
	extracellular matrix	4
	cell cycle	4
	aging	3
	angiogenesis	2
	RNA splicing	1
	response to oxidative stress	1
	DNA repair	1
	Down-Regulated Genes	
	signal transduction	24
	transcription	24
	cell differentiation	20
	cell proliferation	15
	cell cycle	9
	immune response	9
	apoptosis	8
	inflammatory response	8
	regulation of cellular protein metabolic process	6
	angiogenesis	5
	neurogenesis	5
	aging	2
	DNA repair	2
	extracellular matrix	2
	response to oxidative stress	1

[a]The cutoff of *M* value is >2 for up-regulation and <0.5 for down-regulation.

Table 2. Cell Differentiation

gene symbol	gene name	accession no.	fold of change in spiky SPs
Up-Regulated Genes			
Sry	**sex determining region of Chr Y**	**NM_011564**	**7.14**
Spp1	secreted phosphoprotein 1	NM_009263	7.07
Ascl2	achaete-scute complex homologue 2 (Drosophila)	NM_008554	4.27
Tcf23	transcription factor 23	NM_053085	3.96
Onecut2	one cut domain, family member 2	NM_194268	3.82
Emx2	empty spiracles homologue 2 (Drosophila)	NM_010132	3.66
Notch4	notch gene homologue 4 (Drosophila)	NM_010929	3.63
Il2rg	interleukin 2 receptor, gamma chain	NM_013563	3.50
Aspa	aspartoacylase	NM_023113	3.21
Hsf4	heat shock transcription factor 4	NM_011939	3.21
Crygd	crystallin, gamma D	NM_007776	3.05
Terc	telomerase RNA component	NR_001579	3.05
Mib1	mindbomb homologue 1 (Drosophila)	NM_144860	2.78
Olig2	oligodendrocyte transcription factor 2	NM_016967	2.74
Omp	olfactory marker protein	NM_011010	2.71
Dtx1	deltex 1 homologue (Drosophila)	NM_008052	2.68
Sox3	SRY-box containing gene 3	NM_009237	2.67
Il23a	interleukin 23, alpha subunit p19	NM_031252	2.51
Sprr4	small proline-rich protein 4	NM_173070	2.36
Tubd1	tubulin, delta 1	NM_019756	2.28
Lhx2	LIM homeobox protein 2	NM_010710	2.26
Slc1a3	solute carrier family 1 (glial high affinity glutamate transporter), member 3	NM_148938	2.15
Met	met proto-oncogene	NM_008591	2.10
Pdgfrb	platelet derived growth factor receptor, beta polypeptide	NM_001146268	2.10
Ager	advanced glycosylation end product-specific receptor	NM_007425	2.04
Up-Regulated Genes			
Sema5a	sema domain, seven thrombospondin repeats (type 1 and type 1-like), transmembrane domain (TM), and short cytoplasmic domain, (semaphorin) 5A	NM_009154	2.02
Down-Regulated Genes			
Il11ra1	**interleukin 11 receptor, alpha chain 1**	**NM_001172054**	**0.24**
Ntf5	neurotrophin 5	NM_198190	0.31
Mkks	McKusick−Kaufman syndrome protein	NM_021527	0.34
Zic3	zinc finger protein of the cerebellum 3	NM_009575	0.39
Coq7	demethyl-Q 7	NM_009940	0.39
Sprr1b	small proline-rich protein 1B	NM_009265	0.40
Phox2a	paired-like homeobox 2a	NM_008887	0.41
Fabp4	fatty acid binding protein 4, adipocyte	NM_024406	0.42
Trim54	tripartite motif-containing 54	NM_021447	0.42
Gab2	growth factor receptor bound protein 2-associated protein 2	NM_010248	0.42
Pex11a	peroxisomal biogenesis factor 11 alpha	NM_011068	0.43
Acadm	acyl-Coenzyme A dehydrogenase, medium chain	NM_007382	0.43
Azi1	5-azacytidine induced gene 1	NM_009734	0.44
Tcp11	t-complex protein 11	NM_013687	0.44
Lhx5	LIM homeobox protein 5	NM_008499	0.45
Cd3e	CD3 antigen, epsilon polypeptide	NM_007648	0.46
Basp1	brain abundant, membrane attached signal protein 1	NM_027395	0.47
Cxcr4	chemokine (C−X−C motif) receptor 4	NM_009911	0.47
Cd28	CD28 antigen	NM_007642	0.47
Vps33a	vacuolar protein sorting 33A (yeast)	NM_029929	0.48

groups, vehicle, and spiky SP group, in which the vehicle is a deionized water-treated group and the spiky SP group had different concentrations of spiky SP (0.79, 1.58, 3.17, 6.25, 12.5, 25, and 50 μg/mL) treated group. Electrophoretic traces and electropherograms told us that bands for 28S, 18S, and 5.8S rRNA were clearly detected in the total RNA extracted from each group; they exhibited normal patterns in electrophoretic traces (Figure 5A and B), demonstrating that the total RNA extracted from all cells was of sufficient quality for microarray analysis plots.

Figure 5C shows microarray analysis plot summaries of gene expression data on the mouse genome survey, in which 33 315 genes were analyzed for the spiky groups. The microarray analysis plot presents dependences between the log ratio of two variables and the mean values of the same two variables that were analyzed from red (R) and green (G) channels of a single chip to visualize the intensity-dependent ratio of raw microarray data. In our experiment, the G value represents the vehicle group, and the R value represents the spiky groups. The middle line (M = 1) depicts equivalent intensity of R and G, indicating equivalent gene expression between the vehicle and spiky groups. An M value of >2 indicates more than 2-fold up-regulation in gene expression in the spiky group, compared with that in the vehicle group. The location of average gene expression values along the first diagonal in Figure 5C (average intensity vs intensity ratio) shows systematic bias of overall distributions of gene expression.

DISCUSSION

Distribution of the Regulated Genes. To analyze the ontology classification of spiky SP-regulated gene expression in sarcoma 180 cells, we categorized gene lists through functional clustering according to gene ontology (GO) classification using the PANTHER/X ontology online software. On the basis of the cutoffs of M value >2 for up-regulation and <0.5 for down-regulation, 171 were increased, and 181 were down-regulated in the spiky SP group. These results suggest that microarray analysis can identify differences effectively in gene expression resulting from the treatment with the control and the spiky SPs. The PANTHER/X ontology software identified 16 major GO categories in the list of up-regulated transcripts. As shown in Table 1, the largest number of transcripts was associated with signal transduction, followed by cell differentiation, transcription neurogenesis, cell proliferation, and apoptosis. In the list of down-regulated transcripts, the PANTHER/X ontology software identified 15 major GO categories (Table 1) that were generally very similar to the categories of the up-regulated transcripts. In this group, genes involved in signal transduction and transcription were especially highly expressed, followed by those involved in cell differentiation, cell proliferation, cell cycle, immune response, and apoptosis. These results suggest

Table 3. Cell Proliferation

gene symbol	gene name	accession no.	fold of change in spiky SPs
Up-Regulated Genes			
Il1b	**interleukin 1 beta**	**NM_008361**	**8.25**
Ascl2	achaete-scute complex homologue 2 (Drosophila)	NM_008554	4.27
Emx2	empty spiracles homologue 2 (Drosophila)	NM_010132	3.66
Hsf4	heat shock transcription factor 4	NM_011939	3.21
Terc	telomerase RNA component	NR_001579	3.05
Crip2	cysteine rich protein 2	NM_024223	2.56
Ncf1	neutrophil cytosolic factor 1	NM_010876	2.55
Il23a	interleukin 23, alpha subunit p19	NM_031252	2.51
Eif5a2	eukaryotic translation initiation factor 5A2	NM_177586	2.29
Met	met proto-oncogene	NM_008591	2.10
Pdgfrb	platelet derived growth factor receptor, beta polypeptide	NM_001146268	2.10
Ager	advanced glycosylation end product-specific receptor	NM_007425	2.04
Down-Regulated Genes			
Rbp4	**retinol binding protein 4, plasma**	**NM_001159487**	**0.22**
Il11ra1	interleukin 11 receptor, alpha chain 1	NM_001172054	0.24
Hdgfrp3	hepatoma-derived growth factor, related protein 3	NM_013886	0.27
Il18	interleukin 18	NM_008360	0.31
Fabp4	fatty acid binding protein 4, adipocyte	NM_024406	0.42
Gab2	growth factor receptor bound protein 2-associated protein 2	NM_010248	0.42
Prrx2	paired related homeobox 2	NM_009116	0.44
B4galt7	xylosylprotein beta1,4-galactosyltransferase, polypeptide 7 (galactosyltransferase I)	NM_146045	0.44
Lhx5	LIM homeobox protein 5	NM_008499	0.45
Itgb2	integrin beta 2	NM_008404	0.46
Cd3e	CD3 antigen, epsilon polypeptide	NM_007648	0.46
Hsf1	heat shock factor 1	NM_008296	0.46
Cxcr4	chemokine (C−X−C motif) receptor 4	NM_009911	0.47
Cd28	CD28 antigen	NM_007642	0.47
Hyal1	hyaluronoglucosaminidase 1	NM_008317	0.50

Table 4. Apoptosis

gene symbol	gene name	accession no.	fold of change in spiky SPs
Up-Regulated Genes			
Il1b	**interleukin 1 beta**	**NM_008361**	**8.25**
Spp1	secreted phosphoprotein 1	NM_009263	7.07
Uaca	uvealautoantigen with coiled-coil domains and ankyrin repeats	NM_028283	5.18
Terc	telomerase RNA component	NR_001579	3.05
Ncf1	neutrophil cytosolic factor 1	NM_010876	2.55
Bcl7c	B-cell CLL/lymphoma 7C	NM_009746	2.48
Traf3ip2	TRAF3 interacting protein 2	NM_134000	2.36
Rnf130	ring finger protein 130	NM_021540	2.05
Ager	advanced glycosylation end product-specific receptor	NM_007425	2.04
Down-Regulated Genes			
Il18	**interleukin 18**	**NM_008360**	**0.31**
Nr4a1	nuclear receptor subfamily 4, group A, member 1	NM_010444	0.34
Irak3	interleukin-1 receptor-associated kinase 3	NM_028679	0.36
Cd3e	CD3 antigen, epsilon polypeptide	NM_007648	0.46
Nmnat3	nicotinamide nucleotide adenylyltransferase 3	NM_144533	0.46
Cd28	CD28 antigen	NM_007642	0.47
Pdcd7	programmed cell death 7	NM_016688	0.50
P2rx4	purinergic receptor P2X, ligand-gated ion channel 4	NM_011026	0.50

that spiky SPs regulate the expression of genes related to signal transduction, cell differentiation, and regulation of gene expression in sarcoma 180 cells.

Genes with the Highest Up-Regulation and Down-Regulation. To characterize genes showing the highest levels of overexpression, we selected three categories (i.e., cell differentiation, proliferation, and apoptosis) directly related to cell viability from Table 1, and genes showing at least a 2-fold increase in expression were ranked according to their expression levels. Within these cell differentiation categories (Table 2), transcripts with the highest fold increase in the spiky SPs group were *Sry* (7.14-fold), which initiates male sex determination. Moreover, several transcripts, including *Il11ra1*, *Ntf5*, *Mkks*, *Zic3*, and *Coq7*, were expressed at lower levels in the spiky SP group. In the cell proliferation category (Table 3), a dramatic increase in expression was observed for the *Il1b* transcript (8.25-fold) among the up-regulated genes. The information about *Il1b* and *Rbp4* genes was cited from NCBI GenBank. The protein encoded by *Il1b* is a member of the interleukin 1 cytokine family, which is produced by activated macrophages as a proprotein and proteolysis to its active form by *caspase 1* (CASP1/ICE).[57] As an important regulator of the inflammatory response, it has been involved in a variety of cellular activities, including cell proliferation, differentiation, and apoptosis. Rbp4 (Retinol binding protein 4) presents the highest down-regulation in this group. Not only does it belong to the lipocalin family but also carries retinol (vitamin A alcohol) from the liver stores to the peripheral tissues.[58]

Finally, for the up-regulated genes in the apoptosis category (Table 4), *I11b* and *Spp1* were the most highly up-regulated in the spiky SP group, followed by *Uaca*, *Terc*, *Ncf1*, and *Bcl7c.Il18*, *Nr4a1*, and *Irak3* were the most highly down-regulated in the spiky SP group. Interleukin-1 receptor-associated kinase 3 (*Irak3*) is an enzyme encoded by the IRAK3 gene.[59] Members of this family play a vital role in Toll/IL-R immune signal transduction. These results indicate that spiky SP treatment regulates genes involved in cell proliferation, cell differentiation, and apoptosis.

Biological Pathway Analysis. To study the role of genes with the highest expression induced by spiky SP treatment, we used the Kyoto Encyclopedia of Genes and Genomes to analyze three important up-regulated genes: *Spp1*, *Met*, and *Pdgfrb*. The introduction about these genes was cited from NCBI GenBank. *Spp1* (secreted phosphoprotein 1), the protein encoded by this gene, can secrete hydroxyapatite and binds with it with high affinity, and it can attach osteoclasts to the mineralized bone matrix. As a cytokine, the protein can up-regulate expression of interferon-gamma and interleukin-12.[60] The proto-oncogene MET product is the hepatocyte growth factor receptor. It shows tyrosine-kinase activity.[61] As members

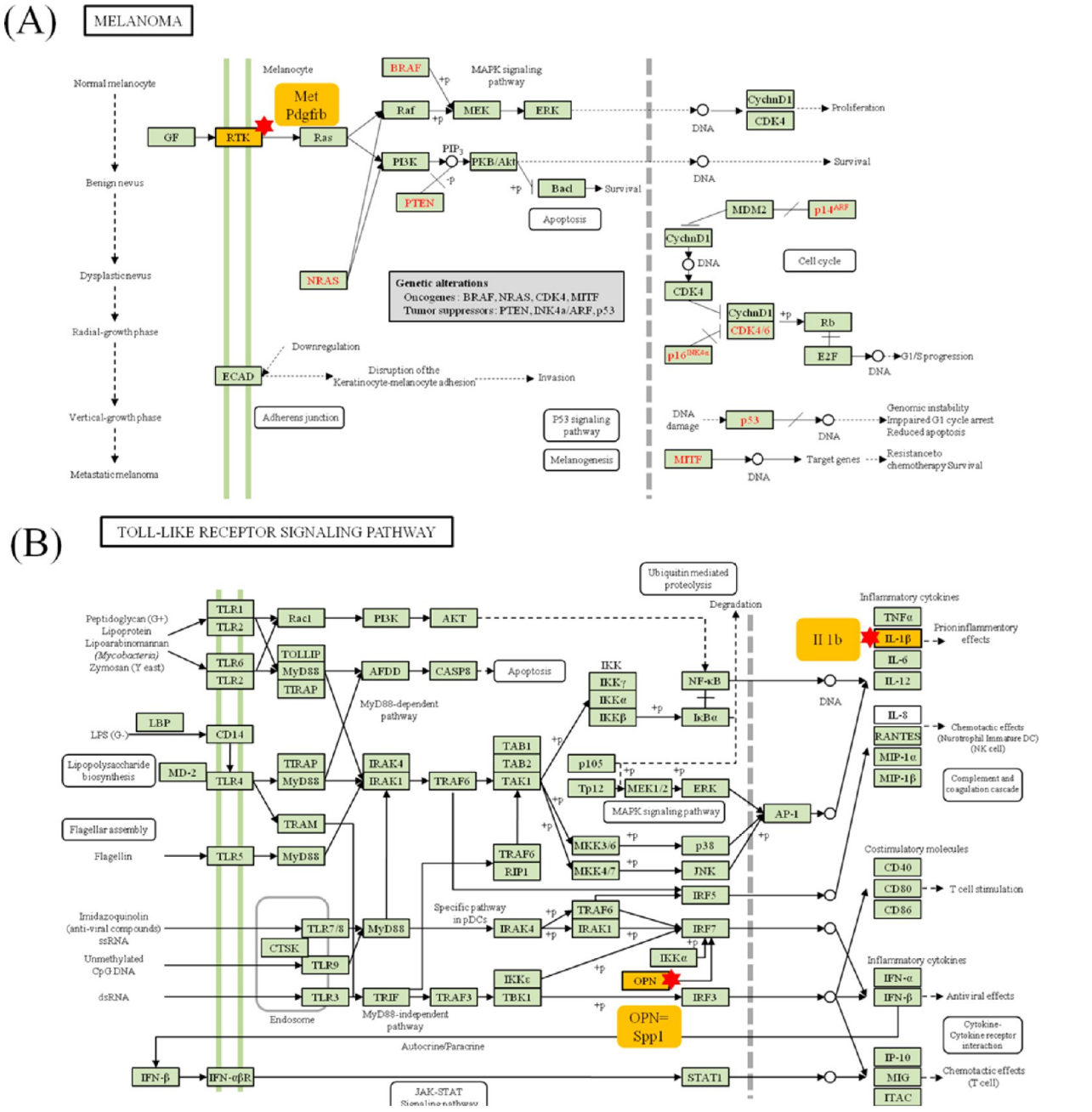

Figure 6. Pathway assignments of important genes based on the spiky SPs. Genes up-regulated in the (A) cell cycle pathway and down-regulated in the (B) TGF-β signaling pathway were determined for spiky SPs. Genes identified in our microarray analysis are labeled using stars.

of the platelet-derived growth factor family, *Pdgfrb* encodes a cell surface of tyrosine kinase receptor.[62] These genes play an important role in focal adhesion and are involved in the synthesis and polymerization of actin through regulation of the focal adhesion kinase and Ras homologue gene family, member A (Figure 6). Moreover, among down-regulated genes, *Il1b*, the gene with the lowest expression level, is closely related to the toll-like receptor-signaling pathway. Peptidoglycan and lipoprotein bind toll-like receptors to stimulate the secretion of cytokines such as tumor necrosis factor α and interleukin (IL)1β, IL-6, and IL-12 via the PI3K signaling pathway.

CONCLUSION

We investigated the influence of spiky Fe_3O_4@Au SPs on cell cytotoxicity and gene expression. The results from our research indicated that different concentrations of spiky SPs showed high cell viability. It suggests that spiky morphology can induce different regulation of gene expression in tumor cells. These findings provide strong evidence that nanostructure not only passively interacts with cells but also actively engages molecular processes essential for the regulation of cell function. Our findings provide useful information for the development of new strategies for cancer treatment.

ASSOCIATED CONTENT

Supporting Information

Optical microscopy and TEM images of sarcoma 180 cells exposed to spiky SPs, rate of early apoptotic cells, and rate of late apoptotic and dead cells exposed to increasing concentrations

dx.doi.org/10.1021/am504632g | ACS Appl. Mater. Interfaces 2014, 6, 19680−19689

(0−50 μg/mL) of magnetic core NPs. This material is available free of charge via the Internet at http://pubs.acs.org.

AUTHOR INFORMATION

Corresponding Authors

*E-mail: dyhwang@pusan.ac.kr (D. Y. Hwang).
*E-mail: jaebeom@pusan.ac.kr (J. Lee). Tel.: (+82)55-350-5298. Fax: (+82)55-350-5299.

Present Address

[⊥]Research Institute & Hospital, National Cancer Center, Goyang 410-769, Republic of Korea; Department of Life Science, Ewha Womans University, Seoul 120-750, Republic of Korea.

Author Contributions

[∥]These authors contributed equally to this work

Notes

The authors declare no competing financial interest.

ACKNOWLEDGMENTS

This work was supported by a 2-Year Research Grant of Pusan National University.

REFERENCES

(1) Vasir, J. K.; Labhasetwar, V. Quantification of the Force of Nanoparticle-cell Membrane Interactions and its Influence on Intracellular Trafficking of Nanoparticles. *Biomaterials* **2008**, *29*, 4244−4252.

(2) Rana, S.; Bajaj, A.; Mout, R.; Rotello, V. M. Monolayer Coated Gold Nanoparticles for Delivery Applications. *Adv. Drug Delivery Rev.* **2012**, *64*, 200−216.

(3) la Rocca, J.; Liu, D.; Lin, W. Nanoscale Metal−Organic Frameworks for Biomedical Imaging and Drug Delivery. *Acc. Chem. Res.* **2011**, *44*, 957−968.

(4) Absolom, D. R.; Zingg, W.; Neumann, A. W. Protein Adsorption to Polymer Particles: Role of Surface Properties. *J. Biomed. Mater. Res.* **1987**, *21*, 161−171.

(5) Haas, T. A.; Plow, E. F. Integrin-Ligarid Interactions: A Year in Review. *Curr. Opin. Cell Biol.* **1994**, *6*, 656−662.

(6) Xu, Z.; Chen, L.; Gu, W.; Gao, Y.; Lin, L.; Zhang, Z.; Xi, Y.; Li, Y. The Performance of Docetaxel-loaded Solid Lipid Nanoparticles Targeted to Hepatocellular Carcinoma. *Biomaterials* **2009**, *30*, 226−232.

(7) Chithrani, B. D.; Ghazani, A. A.; Chan, W. C. W. Determining the Size and Shape Dependence of Gold Nanoparticle Uptake into Mammalian Cells. *Nano Lett.* **2006**, *6*, 662−668.

(8) Chung, T. H.; Wu, S. H.; Yao, M.; Lu, C. W.; Lin, Y. S.; Hung, Y.; Mou, C. Y.; Chen, Y. C.; Huang, D. M. The Effect of Surface Charge on the Uptake and Biological Function of Mesoporous Silica Nanoparticles in 3T3-L1 Cells and Human Mesenchymal Stem Cells. *Biomaterials* **2007**, *28*, 2959−2966.

(9) Champion, J. A.; Mitragotri, S. Role of Target Geometry in Phagocytosis. *Proc. Natl. Acad. Sci. U. S. A.* **2006**, *103*, 4930.

(10) Huang, X.; Teng, X.; Chen, D.; Tang, F.; He, J. The Effect of the Shape of Mesoporous Silica Nanoparticles on Cellular Uptake and Cell Function. *Biomaterials* **2010**, *31*, 438−448.

(11) Zhou, H.; Dong, J.; Deo, V. K.; Park, E. Y.; Lee, J. Detection of Anti-Neospora Antibodies in Bovine Serum by using Spiky Au-CdTe Nanocomplexes. *Sens. Actuators, B* **2012**, *178*, 192−199.

(12) Gratton, S. E. A.; Ropp, P. A.; Pohlhaus, P. D.; Luft, J. C.; Madden, V. J.; Napier, M. E.; DeSimone, J. M. The Effect of Particle Design on Cellular Internalization Pathways. *Proc. Natl. Acad. Sci. U.S.A.* **2008**, *105*, 11613.

(13) Lewinski, N.; Colvin, V.; Drezek, R. Cytotoxicity of Nanoparticles. *Small* **2008**, *4*, 26−49.

(14) Tarantola, M.; Pietuch, A.; Schneider, D.; Rother, J.; Sunnick, E.; Rosman, C.; Pierrat, S.; Sonnichsen, C.; Wegener, J.; Janshoff, A. Toxicity of Gold-nanoparticles: Synergistic Effects of Shape and Surface Functionalization on Micromotility of Epithelial Cells. *Nanotoxicology* **2011**, *5*, 254−268.

(15) Tian, N.; Zhou, Z. Y.; Yu, N. F.; Wang, L. Y.; Sun, S. G. Direct Electrodeposition of Tetrahexahedral Pd Nanocrystals with High-index Facets and High Catalytic Activity for Ethanol Electrooxidation. *J. Am. Chem. Soc.* **2010**, *132*, 7580−7581.

(16) Ming, T.; Feng, W.; Tang, Q.; Wang, F.; Sun, L.; Wang, J.; Yan, C. Growth of Tetrahexahedral Gold Nanocrystals with High-index Facets. *J. Am. Chem. Soc.* **2009**, *131*, 16350−16351.

(17) Zhang, J.; Langille, M. R.; Personick, M. L.; Zhang, K.; Li, S.; Mirkin, C. A. Concave Cubic Gold Nanocrystals with High-Index Facets. *J. Am. Chem. Soc.* **2010**, *132*, 14012−14014.

(18) Lu, C. L.; Prasad, K. S.; Wu, H. L.; Ho, J. a. A.; Huang, M. H. Au Nanocube-Directed Fabrication of Au-Pd Core-Shell Nanocrystals with Tetrahexahedral, Concave Octahedral, and Octahedral Structures and their Electrocatalytic Activity. *J. Am. Chem. Soc.* **2010**, *132*, 14546−14553.

(19) Yu, Y.; Zhang, Q.; Liu, B.; Lee, J. Y. Synthesis of Nanocrystals with Variable High-Index Pd Facets through the Controlled Heteroepitaxial Growth of Trisoctahedral Au Templates. *J. Am. Chem. Soc.* **2010**, *132*, 18258−18265.

(20) Wang, F.; Li, C.; Sun, L. D.; Wu, H.; Ming, T.; Wang, J.; Yu, J. C.; Yan, C. H. Heteroepitaxial Growth of High-Index-Faceted Palladium Nanoshells and their Catalytic Performance. *J. Am. Chem. Soc.* **2010**, *133*, 1106−1111.

(21) Zhou, Z.-Y.; Huang, Z.-Z.; Chen, D.-J.; Wang, Q.; Tian; Sun, S.-G. High−Index Faceted Platinum Nanocrystals Supported on Carbon Black as Highly Efficient Catalysts for Ethanol Electrooxidation. *Angew. Chem., Int. Ed.* **2010**, *49*, 411−414.

(22) Ma, Y.; Kuang, Q.; Jiang, Z.; Xie, Z.; Huang, R.; Zheng, L. Synthesis of Trisoctahedral Gold Nanocrystals with Exposed High−Index Facets by a Facile Chemical Method. *Angew. Chem., Int. Ed.* **2008**, *47*, 8901−8904.

(23) Kim, D. Y.; Im, S. H.; Park, O. O. Synthesis of Tetrahexahedral Gold Nanocrystals with High-index Facets. *Cryst. Growth Des.* **2010**, *10*, 3321−3323.

(24) Gong, J.; Li, G.; Tang, Z. Self-assembly of Noble Metal Nanocrystals: Fabrication, Optical Property, and Application. *Nano Today* **2012**, *7*, 564−585.

(25) Lyon, J. L.; Fleming, D. A.; Stone, M. B.; Schiffer, P.; Williams, M. E. Synthesis of Fe Oxide Core/Au Shell Nanoparticles by Iterative Hydroxylamine Seeding. *Nano Lett.* **2004**, *4*, 719−723.

(26) Brullot, W.; Valev, V. K.; Verbiest, T. Magnetic-Plasmonic Nanoparticles for the Life Sciences: Calculated Optical Properties of Hybrid Structures. *Nanomedicine (N. Y., NY, U. S.)* **2012**, *8*, 559−568.

(27) Li, Z.; Cheng, E.; Huang, W.; Zhang, T.; Yang, Z.; Liu, D.; Tang, Z. Improving the Yield of Mono-DNA-Functionalized Gold Nanoparticles through Dual Steric Hindrance. *J. Am. Chem. Soc.* **2011**, *133*, 15284−15287.

(28) Li, Z.; Zhu, Z.; Liu, W.; Zhou, Y.; Han, B.; Gao, Y.; Tang, Z. Reversible Plasmonic Circular Dichroism of Au Nanorod and DNA Assemblies. *J. Am. Chem. Soc.* **2012**, *134*, 3322−3325.

(29) Wang, J.; Gong, J.; Xiong, Y.; Yang, J.; Gao, Y.; Liu, Y.; Lu, X.; Tang, Z. Shape-dependent Electrocatalytic Activity of Monodispersed Gold Nanocrystals Toward Glucose Oxidation. *Chem. Commun.* **2011**, *47*, 6894−6896.

(30) Niemeyer, C. M. Nanoparticles, Proteins, and Nucleic Acids: Biotechnology Meets Materials Science. *Angew. Chem., Int. Ed.* **2001**, *40*, 4128−4158.

(31) Zhou, H.; Zou, F.; Koh, K.; Lee, J. Multifunctional Magnetoplasmonic Nanomaterials and Their Biomedical Applications. *J. Biomed. Nanotechnol.* **2014**, *10*, 2921−2949.

(32) Riepl, M.; Östblom, M.; Lundström, I.; Svensson, S. C.; Denier van der Gon, A.; Schäferling, M.; Liedberg, B. Molecular Gradients: an Efficient Approach for Optimizing the Surface Properties of Biomaterials and Biochips. *Langmuir* **2005**, *21*, 1042−1050.

(33) Cheng, L. C.; Huang, J. H.; Chen, H. M.; Lai, T. C.; Yang, K. Y.; Liu, R. S.; Hsiao, M.; Chen, C. H.; Her, L. J.; Tsai, D. P. Seedless,

Silver-induced Synthesis of Star-shaped Gold/Silver Bimetallic Nanoparticles as High Efficiency Photothermal Therapy Reagent. *J. Mater. Chem.* **2012**, *22*, 2244−2253.
(34) Kouassi, G. K.; Irudayaraj, J. Magnetic and Gold-coated Magnetic Nanoparticles as a DNA Sensor. *Anal. Chem.* **2006**, *78*, 3234−3241.
(35) Robinson, I.; Tung, L. D.; Maenosono, S.; W+ñlti, C.; Thanh, N. T. Synthesis of Core-Shell Gold Coated Magnetic Nanoparticles and their Interaction with Thiolated DNA. *Nanoscale* **2010**, *2*, 2624−2630.
(36) Godin, B.; Tasciotti, E.; Liu, X.; Serda, R. E.; Ferrari, M. Multistage Nanovectors: from Concept to Novel Imaging Contrast Agents and Therapeutics. *Acc. Chem. Res.* **2011**, *44*, 979−989.
(37) Tassa, C.; Shaw, S. Y.; Weissleder, R. Dextran-coated Iron Oxide Nanoparticles: A Versatile Platform for Targeted Molecular Imaging, Molecular Diagnostics, and Therapy. *Acc. Chem. Res.* **2011**, *44*, 842−852.
(38) Yoo, D.; Lee, J. H.; Shin, T. H.; Cheon, J. Theranostic Magnetic Nanoparticles. *Acc. Chem. Res.* **2011**, *44*, 863−874.
(39) Xia, W.; Song, H. M.; Wei, Q.; Wei, A. Differential Response of Macrophages to Core-Shell Fe3O4@Au Nanoparticles and Nanostars. *Nanoscale* **2012**, *4*, 7143−7148.
(40) Liang, P.; Pardee, A. B. Differential Display of Eukaryotic Messenger RNA by Means of the Polymerase Chain Reaction. *Science* **1992**, *257*, 967−971.
(41) Shimkets, R. A.; Lowe, D. G.; Tai, J. T.-N.; Sehl, P.; Jin, H.; Yang, R.; Predki, P. F.; Rothberg, B. E.; Murtha, M. T.; Roth, M. E. Gene Expression Analysis by Transcript Profiling Coupled to a Gene Database Query. *Nat. Biotechnol.* **1999**, *17*, 798−803.
(42) Golub, T. R.; Slonim, D. K.; Tamayo, P.; Huard, C.; Gaasenbeek, M.; Mesirov, J. P.; Coller, H.; Loh, M. L.; Downing, J. R.; Caligiuri, M. A. Molecular Classification of Cancer: Class Discovery and Class Prediction by Gene Expression Monitoring. *Science* **1999**, *286*, 531−537.
(43) Marton, M. J.; DeRisi, J. L.; Bennett, H. A.; Iyer, V. R.; Meyer, M. R.; Roberts, C. J.; Stoughton, R.; Burchard, J.; Slade, D.; Dai, H. Drug Target Validation and Identification of Secondary Drug Target Effects using DNA Microarrays. *Nat. Med. (N. Y., NY, U. S.)* **1998**, *4*, 1293−1301.
(44) Nuwaysir, E. F.; Bittner, M.; Trent, J.; Barrett, J. C.; Afshari, C. A. Microarrays and Toxicology: the Advent of Toxicogenomics. *Mol. Carcinog.* **1999**, *24*, 153−159.
(45) Zhou, H.; Kim, J. P.; Bahng, J. H.; Kotov, N. A.; Lee, J. Self-Assembly Mechanism of Spiky Magnetoplasmonic Supraparticles. *Adv. Funct. Mater.* **2014**, *24*, 1439−1448.
(46) Xia, Y.; Tang, Z. Monodisperse Inorganic Supraparticles: Formation Mechanism, Properties and Applications. *Chem. Commun. (Cambridge, U. K.)* **2012**, *48*, 6320−6336.
(47) Xia, Y.; Nguyen, T. D.; Yang, M.; Lee, B.; Santos, A.; Podsiadlo, P.; Tang, Z.; Glotzer, S. C.; Kotov, N. A. Self-assembly of Self-limiting Monodisperse Supraparticles from Polydisperse Nanoparticles. *Nat. Nanotechnol.* **2011**, *6*, 580−587.
(48) Nigam, S.; Barick, K. C.; Bahadur, D. Development of Citrate-stabilized Fe3O4 Nanoparticles: Conjugation and Release of Doxorubicin for Therapeutic Applications. *J. Magn. Magn. Mater.* **2011**, *323*, 237−243.
(49) Zhou, H.; Lee, J.; Park, T. J.; Lee, S. J.; Park, J. Y.; Lee, J. Ultrasensitive DNA Monitoring by Au−Fe3O4 Nanocomplex. *Sens. Actuators, B* **2012**, *163*, 224−232.
(50) Ha, S. E.; Shin, D. H.; Do Kim, H.; Shim, S. M.; Kim, H. S.; Kim, B. H.; Lee, J. S.; Park, J. K. Effects of Ginsenoside Rg2 on the Ultraviolet B-induced DNA Damage Responses in HaCaT Cells. *Naunyn-Schmiedeberg's Arch. Pharmacol.* **2010**, *382*, 89−101.
(51) Yeo, M. K.; Kim, H. E. Gene Expression in Zebrafish Embryos Following Exposure to TiO2 Nanoparticles. *Mol. Cell. Toxicol.* **2010**, *6*, 97−104.
(52) Lee, J.; Kim, H. Y.; Zhou, H.; Hwang, S.; Koh, K.; Han, D. W.; Lee, J. Green Synthesis of Phytochemical-stabilized Au Nanoparticles under Ambient Conditions and their Biocompatibility and Antioxidative Activity. *J. Mater. Chem.* **2011**, *21*, 13316−13326.
(53) Nativo, P.; Prior, I. A.; Brust, M. Uptake and Intracellular Fate of Surface-Modified Gold Nanoparticles. *ACS Nano* **2008**, *2*, 1639−1644.
(54) AshaRani, P. V.; Low Kah Mun, G.; Hande, M. P.; Valiyaveettil, S. Cytotoxicity and Genotoxicity of Silver Nanoparticles in Human Cells. *ACS Nano* **2008**, *3*, 279−290.
(55) Soenen, S. J.; Manshian, B.; Montenegro, J. M.; Amin, F.; Meermann, B.; Thiron, T.; Cornelissen, M.; Vanhaecke, F.; Doak, S.; Parak, W. J. Cytotoxic Effects of Gold Nanoparticles: A Multiparametric Study. *ACS Nano* **2012**, *6*, 5767−5783.
(56) Pan, Y.; Neuss, S.; Leifert, A.; Fischler, M.; Wen, F.; Simon, U.; Schmid, G.; Brandau, W.; Jahnen-Dechent, W. Size-Dependent Cytotoxicity of Gold Nanoparticles. *Small* **2007**, *3*, 1941−1949.
(57) IL1B interleukin 1, beta. http://www.ncbi.nlm.nih.gov/gene/3553, 2014.
(58) RBP4 retinol binding protein 4, plasma. http://www.ncbi.nlm.nih.gov/gene/5950, 2014.
(59) IRAK3 interleukin-1 receptor-associated kinase 3. http://www.ncbi.nlm.nih.gov/gene/11213, 2014.
(60) SPP1 secreted phosphoprotein 1. http://www.ncbi.nlm.nih.gov/gene/6696, 2014.
(61) MET proto-oncogene, receptor tyrosine kinase. http://www.ncbi.nlm.nih.gov/gene/4233, 2014.
(62) PDGFRB platelet-derived growth factor receptor, beta polypeptide. http://www.ncbi.nlm.nih.gov/gene/5159, 2014.